JOURNAL OF GUIDANCE, CONTROL, AND DYNAMICS
Vol. 25, No. 5, September–October 2002

Optimal Control of Interplanetary Trajectories Using Electrical Propulsion with Discrete Thrust Levels

A. Axelrod* and M. Guelman†
Technion—Israel Institute of Technology, 32000 Haifa, Israel
and
D. Mishne‡
RAFAEL Armament Development Authority, Ltd., 31021 Haifa, Israel

A solution is proposed to the optimal closed-loop trajectory control of interplanetary missions, with an electric propulsion system that provides discrete thrust levels. The solution is either suitable to the case of the discrete multilevel electrical engine or to a cluster of several unidirectional engines. The objective is to guide the spacecraft from an initial state to a final state (position and velocity) at an exact given time, with minimum fuel expenditure. The optimization is based on the approach of neighboring optimal trajectory: Given a nominal trajectory (close to, but not necessarily the optimal one), the objective is to control the spacecraft along an optimal neighboring trajectory. In this approach, when a deviation from the planned trajectory is developed, a new neighboring optimal trajectory is calculated to obtain the required end condition, while beginning at the current point. Using this approach, we assure lower fuel consumption, when compared to another control policy that tries to maintain, uncompromisingly, a nominal optimal trajectory. The development of the control law for this problem is presented. An efficient algorithm for the numerical solution of the optimal controller is proposed and demonstrated for two examples: correction of satellite orbit around the moon and an interplanetary rendezvous mission to Mercury.

Introduction

THE potential of electrical propulsion systems for future interplanetary missions has been well recognized.[1] This propulsion system, which is characterized by the variable exhaust velocity and limited power, produces low thrust with high specific impulse. For efficient use, an optimal trajectory is desired. In most cases, the objective is to guide the spacecraft from an initial state to a final state (position and velocity), with minimum fuel expenditure. Optimal trajectory analyses of such systems have been discussed in several comprehensive works, such as that of Marec.[2] Once an optimal trajectory is generated, the problem is to apply proper control logic such that the spacecraft follows the optimal trajectory, in the presence of real-world disturbances. Therefore, a closed-loop controller is desired. Gipsman et al.[3] developed a closed-loop optimal control law for the fixed time rendezvous problem, for an unbounded continuous controller. This solution enabled an analytical determination of the optimal control law at each time step. Advanced analysis should consider practical issues, such as upper and lower bounds on the thrust levels. Carter[4] presented a solution for the rendezvous problem with a continuous bounded controller. Carter and Pardis[5] extended the work for the case where the controller has both upper and lower bounds. To avoid saturation, they proposed the use of multiple engines, where each one has continuous thrust bounded by upper and lower limits. A criterion for their efficient use was developed.

Another practical issue is that electrical engines perform efficiently when they operate at a fixed thrust level.[6] In this paper, we introduce and investigate this practical issue. To follow the desired trajectory, one possible solution is to employ several engines. The controller, thus, is able to provide discrete magnitude levels, and an appropriate control law is desired. The purpose of this paper is to develop a closed-loop control strategy for such missions. Given a nominal trajectory (close to, but not necessarily the optimal one), the objective is to control the spacecraft along an optimal neighboring trajectory, using a discrete multilevel engine or a cluster of several unidirectional engines.

Received 27 April 2001; revision received 21 February 2002; accepted for publication 22 February 2002.

*Graduate Student, Faculty of Aerospace Engineering; currently Research Engineer, Missile Division, RAFAEL, Ltd., 31021 Haifa, Israel.
†Professor and Head, Asher Space Research Institute, Faculty of Aerospace Engineering. Member AIAA.
‡Senior System Engineer, Missile Division. Associate Fellow AIAA.

Statement of the Problem

The basic equation of motion for a spacecraft in an interplanetary mission, assuming the central force field of the sun only, is

$$\ddot{\boldsymbol{r}} = -(\mu/r^3)\boldsymbol{r} + \boldsymbol{f} \tag{1}$$

with the initial conditions $\boldsymbol{r}(t=0)$ and $\dot{\boldsymbol{r}}(t=0)$, where $\boldsymbol{f}$ is the control acceleration, which is produced by a discrete multilevel electrical engine or a cluster of several unidirectional engines. The control parameters are then the direction and the level of the thrust. We deal here with a planar trajectory. The initial and the terminal orbital planes are the same, and no out-of-plane disturbance exists.

The equations of motion in polar sun-centered coordinates r and θ are

$$\dot{r} = v_r, \qquad \dot{\theta} = v_\theta/r, \qquad \dot{v}_r = -(\mu/r^2) + v_\theta^2/r + f_r$$
$$\dot{v}_\theta = -(v_r v_\theta/r) + f_\theta \tag{2}$$

We assume that we have a given nominal trajectory, which is close to the optimal one, from an initial state to a final state. The control problem is to find the optimal controller (optimal in the sense of minimum fuel) that brings the spacecraft from a point near the optimal trajectory to the desired final state at a desired final time. We assume that all of the state variables are measured and that the engine can provide N discrete thrust levels.

Development of Control Law for Multilevel Engine

The nonlinear equations of motion of the spacecraft can be written in the general form

$$\dot{\boldsymbol{X}}(t) = f_1[\boldsymbol{X}(t), \boldsymbol{V}(t)], \qquad \dot{\boldsymbol{V}}(t) = f_2[\boldsymbol{X}(t), \boldsymbol{V}(t)] + \boldsymbol{U} \tag{3}$$

where $\boldsymbol{X}(t)$ and $\boldsymbol{V}(t)$ are the position and the velocity, respectively. $\boldsymbol{U}$ is the control variable (the thrust acceleration vector). The

magnitude of the control variable is bounded by the value b. $U = |\boldsymbol{U}|$ has N discrete positive values, as well as the value $U = 0$. We denote the group of possible control values by U_{b-N}. In the case where $b \to \infty$, we have an unbounded controller U_∞.

We assume that a nominal trajectory $[\boldsymbol{X}_{\text{nom}}(t), \boldsymbol{V}_{\text{nom}}(t)]$ with the proper unbounded controller $U_{\text{nom}} \in U_\infty$ is given. We then define a neighboring trajectory $[\boldsymbol{X}(t) = \boldsymbol{X}_{\text{nom}}(t) + \boldsymbol{x}(t), \boldsymbol{V}(t) = \boldsymbol{V}_{\text{nom}}(t) + \boldsymbol{v}(t)]$ with the controller $\boldsymbol{U}(t) = \boldsymbol{U}_{\text{nom}}(t) + \boldsymbol{u}(t)$. The perturbed linear equations of motion of the neighboring trajectory are

$$\dot{\boldsymbol{y}} = A(t)\boldsymbol{y} + B(t)\boldsymbol{u}, \qquad \boldsymbol{y}(t_0) = \boldsymbol{y}_0 \tag{4}$$

where $\boldsymbol{u}(t)$ is the perturbed controller and $\boldsymbol{y} = [\boldsymbol{x}^T, \boldsymbol{v}^T]^T$ is the resulted perturbed state vector. The matrices $A(t)$ and $B(t)$ are the Jacobian matrices calculated along the nominal trajectory.

The control problem is to find the control variable $\boldsymbol{u}(t)$ such that the spacecraft is guided from the initial state to the final state at a specified time, with minimum fuel expenditure. For an electric limited power engine, the fuel expenditure is proportional to the integral of the square of the thrust acceleration. The cost function is then

$$J[\boldsymbol{U}(t)] = \frac{1}{2}\int_{t_0}^{t_f} \boldsymbol{U}(t)^T \boldsymbol{U}(t)\,\mathrm{d}t \tag{5}$$

subject to $\{\boldsymbol{U} : |\boldsymbol{U}| = |\boldsymbol{U}_{\text{nom}} + \boldsymbol{u}| \in U_{b-N}\}$.

The optimization problem is solved using Pontryagin's minimum principle (see Ref. 7). The Hamiltonian is

$$H = \tfrac{1}{2}\boldsymbol{U}^T\boldsymbol{U} + \boldsymbol{\lambda}^T(A\boldsymbol{y} + B\boldsymbol{u}) = \tfrac{1}{2}\boldsymbol{U}^T\boldsymbol{U} + \boldsymbol{\lambda}^T A\boldsymbol{y} + \boldsymbol{\lambda}^T B\boldsymbol{U} - \boldsymbol{\lambda}^T B\boldsymbol{U}_{\text{nom}} \tag{6}$$

where $\boldsymbol{\lambda}(t)$ is the vector of the Lagrange multipliers.

The necessary conditions for the optimal controller are fulfilled for $\boldsymbol{U}(t) \in U_{b-N}$ that minimizes the Hamiltonian (6), subject to the equations of motion (4) and with the terminal condition $\boldsymbol{y}(t_f) = \boldsymbol{y}_f$. The part of the Hamiltonian that is a function of the control $\boldsymbol{U}$ is

$$L(\boldsymbol{U}) = \tfrac{1}{2}\boldsymbol{U}^T\boldsymbol{U} + \boldsymbol{P}^T\boldsymbol{U} \tag{7}$$

where $\boldsymbol{P}$ is the primer vector defined by $\boldsymbol{P}(t) = B^T\boldsymbol{\lambda}$.

The controller is written as $\boldsymbol{U} = U\boldsymbol{e}_u$, where $U = |\boldsymbol{U}|$ is the magnitude of the controller and $\boldsymbol{e}_u = \boldsymbol{U}/|\boldsymbol{U}|$ is its direction. The Hamiltonian is then

$$L(\boldsymbol{e}_u, U) = \tfrac{1}{2}U^2 + \boldsymbol{P}^T\boldsymbol{e}_u U \tag{8}$$

The direction of the optimal control vector is given by

$$\boldsymbol{e}_u = -(\boldsymbol{P}/|\boldsymbol{P}|) = -(\boldsymbol{P}/p) \tag{9}$$

Hence, $L[\,p(t), U] = \frac{1}{2}U^2 - p(t)\,U$.

The magnitude of the control vector achieves only discrete values between 0 and b. The possible values that minimize the Hamiltonian are given by

$$U = \begin{cases} b, & p(t) \geq b \\ U_{\text{close}}, & \tfrac{1}{2}U_1 < p(t) < b \\ 0, & p(t) \leq \tfrac{1}{2}U_1 \end{cases} \tag{10}$$

If $p(t)$ is equal to the midvalue between U_i and U_{i+1} for a nonzero time interval, then the optimal solution is a chatter between the close possible values (U_i and U_{i+1}). The frequency of this chatter is theoretically infinity, but practically it is limited by the highest possible switching rate.

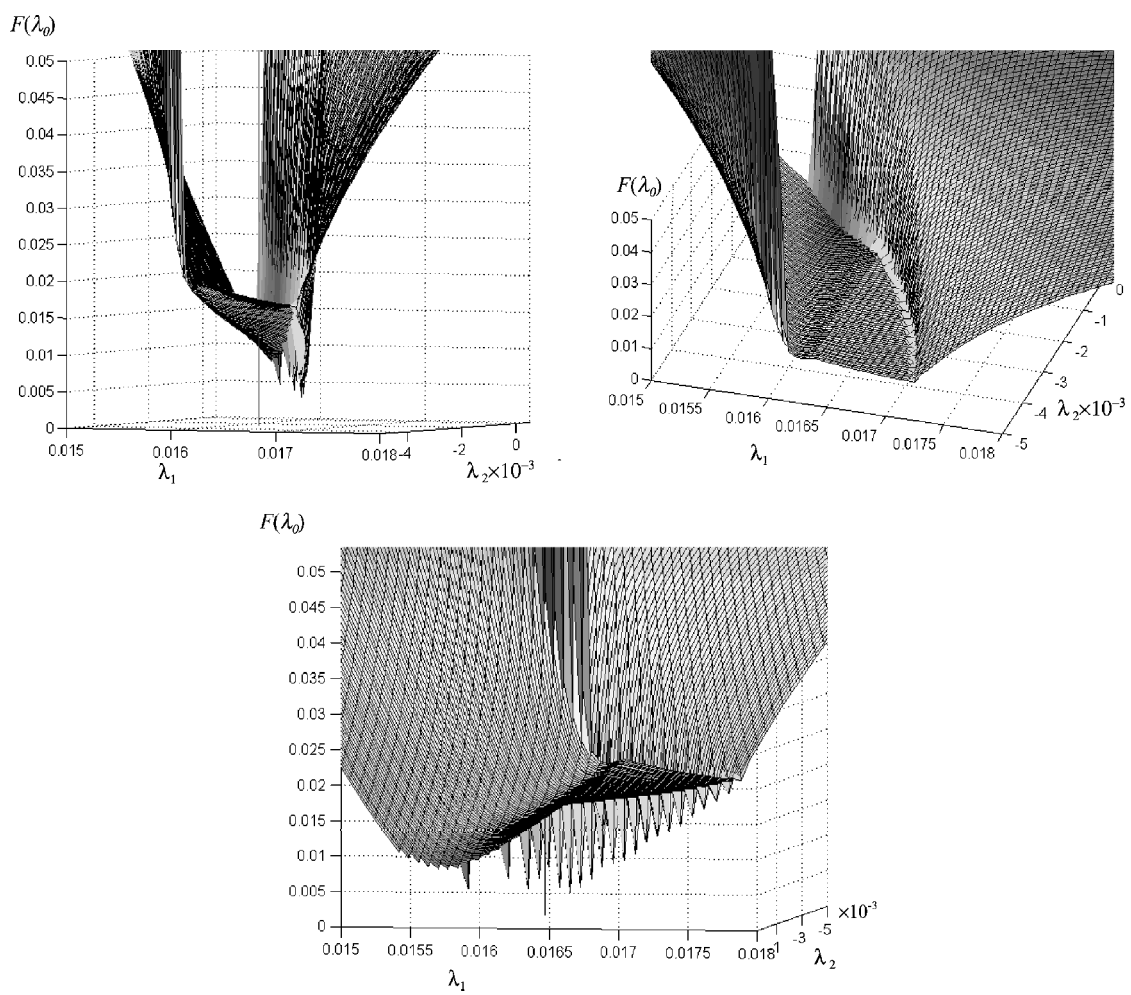

Fig. 1 Typical views of the function $F[\lambda(t_0)]$.

Hence, the optimal control vector is given by

$$U(t) = \begin{cases} -(P/p)b, & p(t) \geq b \\ -(P/p)U_{\text{close}}, & \frac{1}{2}U_1 < p(t) < b \\ 0, & p(t) \leq \frac{1}{2}U_1 \end{cases} \tag{11}$$

where U_{close} is the value of control level U_i that is the closest to the value $p(t)$. To complete the solution, the vector $\boldsymbol{P}$ should be determined. Because $\boldsymbol{P}(t) = B^T\boldsymbol{\lambda}$, we need to determine the vector $\boldsymbol{\lambda}$ along the trajectory. Using the Euler–Lagrange equation $\dot{\boldsymbol{\lambda}}^T = -(\partial H/\partial \boldsymbol{y})$ and the Hamiltonian (6), we get

$$\dot{\boldsymbol{\lambda}} = -A^T\boldsymbol{\lambda} \tag{12}$$

The solution is

$$\boldsymbol{\lambda}(t) = \Phi^{(\lambda)}(t, t_0)\boldsymbol{\lambda}(t_0) \tag{13}$$

where $\Phi^{(\lambda)}$ is the transition matrix that satisfies the equation

$$\dot{\Phi}^{(\lambda)}(t, t_0) = -A(t)^T\Phi^{(\lambda)}(t, t_0) \tag{14}$$

with the initial condition $\Phi^{(\lambda)}(t_0, t_0) = I$. This matrix can be precalculated along the nominal trajectory.

The solution of the equations of motion (4) is given by

$$y(t) = \Phi(t, t_0)y(t_0) + \int_{t_0}^{t} \Phi(t, \tau)Bu(\tau)\,\mathrm{d}\tau \tag{15}$$

where the transition matrix $\Phi(t, t_0)$ is related to the transition matrix $\Phi^{(\lambda)}(t, t_0)$ by

$$\Phi(t, t_0) = \left[\Phi^{(\lambda)}(t, t_0)\right]^{-T} \tag{16}$$

Substituting $u(t) = \boldsymbol{U}(t) - \boldsymbol{U}_{\text{nom}}(t)$, we get

$$\boldsymbol{y}(t) = \Phi(t, t_0)\boldsymbol{y}(t_0) + \boldsymbol{C}(t) - \boldsymbol{n}(t) \tag{17}$$

where $\boldsymbol{C}(t)$ and $\boldsymbol{n}(t)$ are the integrals

$$\boldsymbol{C}(t) = \int_{t_0}^{t} \Phi(t, \tau)B\boldsymbol{U}(\tau)\,\mathrm{d}\tau$$

$$\boldsymbol{n}(t) = \int_{t_0}^{t} \Phi(t, \tau)B\boldsymbol{U}_{\text{nom}}(\tau)\,\mathrm{d}\tau \tag{18}$$

The terminal condition is now used. Solving for $\boldsymbol{y}(t_0)$ from Eq. (17) and requiring $\boldsymbol{y}(t_f) = \boldsymbol{y}_f$, we get the terminal state as a function of the current state $\boldsymbol{y}(t)$:

$$\Phi(t_f, t)\boldsymbol{y}(t) + \tilde{\boldsymbol{C}}(t) - \tilde{\boldsymbol{n}}(t) = \boldsymbol{y}_f \tag{19}$$

where

$$\tilde{\boldsymbol{C}}(t) = \boldsymbol{C}(t_f) - \Phi(t_f, t)\boldsymbol{C}(t), \qquad \tilde{\boldsymbol{n}}(t) = \boldsymbol{n}(t_f) - \Phi(t_f, t)\boldsymbol{n}(t) \tag{20}$$

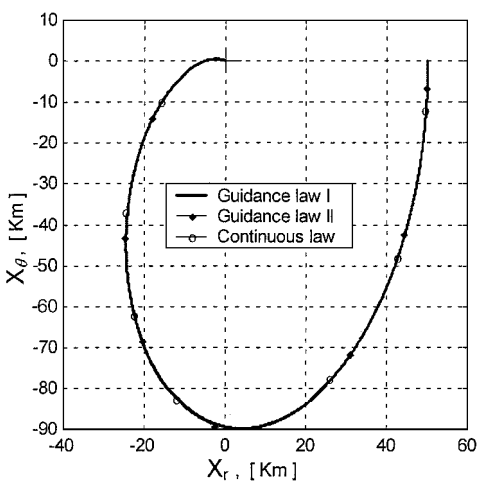

Position deviations

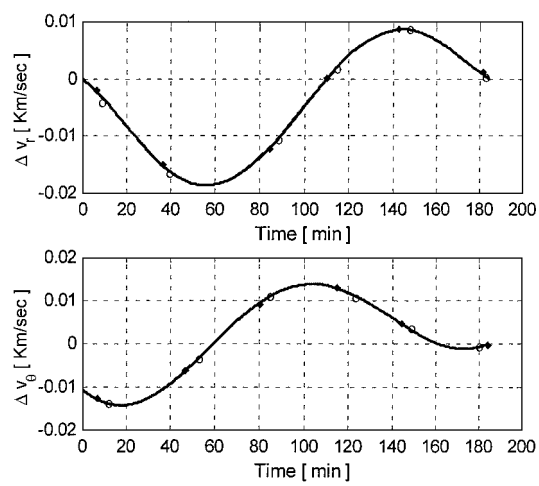

Velocity deviations

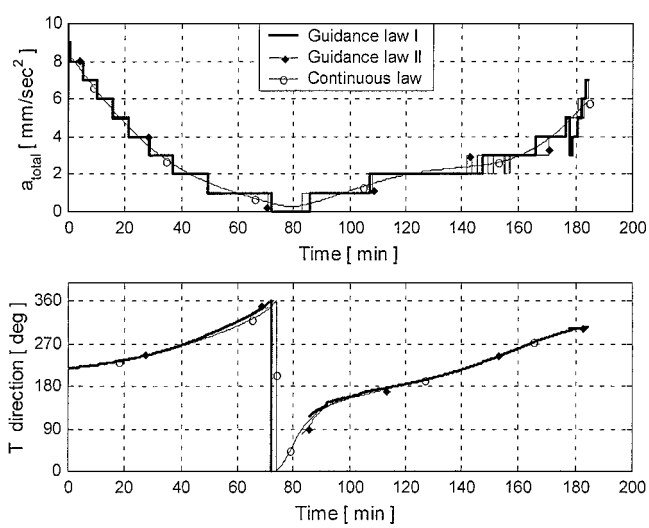

Control magnitude and direction

Fig. 2 Correction of satellite orbit around the moon, $N = 10$.

From Eqs. (18) and (19) it is clear that the matrix $\tilde{\boldsymbol{C}}(t)$ can be calculated at each time step, by the use of the nominal trajectory and the current state measurements.

By substituting $\boldsymbol{P}(t) = B^T \Phi^{-T}(t, t_0)\lambda(t_0)$ into the controller equation (11), we get the controller as a function of the initial value of the Lagrange multipliers vector:

$$U[t, \lambda(t_0)] = \begin{cases} -\dfrac{B^T \Phi^{-T}(t, t_0)\lambda(t_0)}{|B^T \Phi^{-T}(t, t_0)\lambda(t_0)|} b, & |p(t)| \geq b \\ -\dfrac{B^T \Phi^{-T}(t, t_0)\lambda(t_0)}{|B^T \Phi^{-T}(t, t_0)\,\lambda(t_0)|} U_{\text{close}}, & \dfrac{1}{2}U_1 < |p(t)| < b \\ 0, & |p(t)| \leq \dfrac{1}{2}U_1 \end{cases} \quad (21)$$

Next, the value $\boldsymbol{\lambda}(t_0)$ should be determined. Combining controller (21) with Eqs. (18) and (19), we get

$$\tilde{\boldsymbol{C}}[t, \boldsymbol{\lambda}(t_0)] = \boldsymbol{y}_f + \tilde{\boldsymbol{n}}(t) - \Phi(t_f, t)\boldsymbol{y}(t) \quad (22)$$

where $\boldsymbol{y}(t)$ is the measured deviations of the trajectory (position and velocity) from the nominal one. Solving Eq. (22) for $\boldsymbol{\lambda}(t_0)$ as a function of the current time t and substituting into Eq. (21) yields the closed-loop control law.

The actual solution of the preceding equation for $\boldsymbol{\lambda}(t_0)$ is performed iteratively through the search of the minimum of the function

$$\min_{\lambda(t_0)}\{F[\boldsymbol{\lambda}(t_0)] = |\tilde{\boldsymbol{C}}[t, \boldsymbol{\lambda}(t_0)] - \boldsymbol{Z}(t)|\} \quad (23)$$

where $\boldsymbol{Z}(t) = \boldsymbol{y}_f + \tilde{\boldsymbol{n}}(t) - \Phi(t_f, t)\boldsymbol{y}(t)$ and $-Z(t)$ is identified with the zero effort miss at the given instant t, that is, the miss in position and velocity that is expected if no control effort is applied from the moment t to t_f.

The solution is performed by using the simulated annealing method.[8] This method, which was found to be very effective, is further explained in the Appendix.

Behavior of Controller Toward End of Mission

From Eqs. (18) and (20), we get

$$\tilde{C}(t) = \int_t^{t_f} \Phi(t_f, \tau) B U(\tau)\, \mathrm{d}\tau$$

When $t \to t_f$, for any bounded U, $\tilde{C}(t) \to 0$. To fulfill Eq. (22), we require $\tilde{C}(t) = Z(t)$. Then any change in $Z(t)$ as a result of a new measurement may cause a significant change in $U(t)$. The controller might chatter and skip between the extreme values. This will be further demonstrated by the numerical examples in the sequel.

Special Cases

In addition to the controller with N levels, two special cases are discussed: 1) the continuous bounded controller ($N \to \infty$) and bound b and 2) the continuous unbounded controller ($N \to \infty$ and $b \to \infty$).

Continuous Bounded Controller

For the continuous case we have $U_{\text{close}} = p(t)$. The control law is then

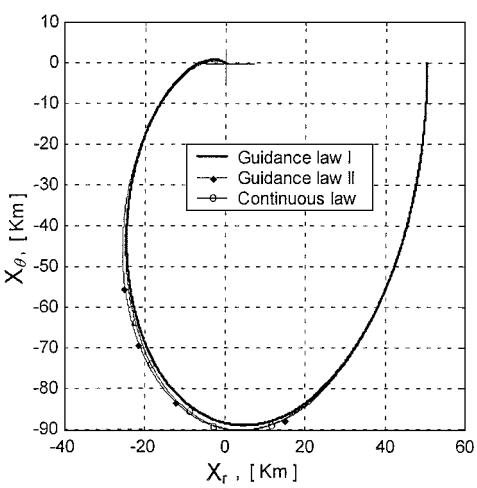

Position deviations

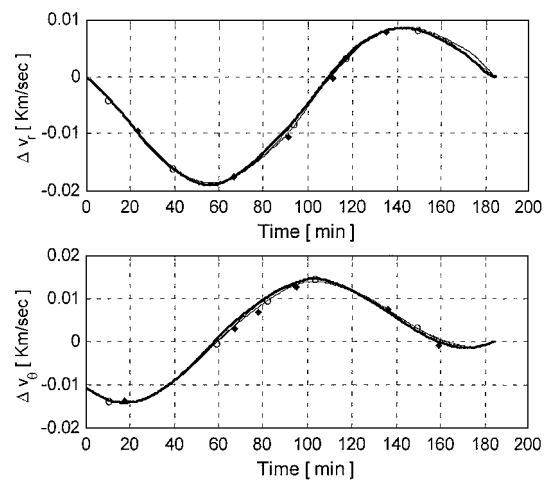

Velocity deviations

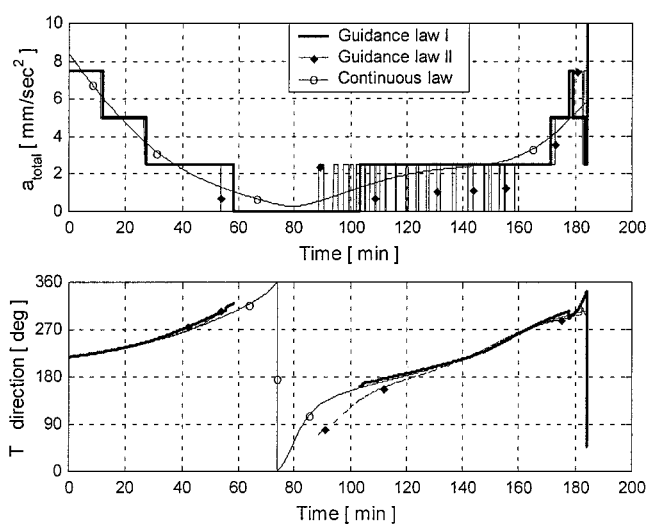

Control magnitude and direction

Fig. 3 Correction of satellite orbit around the moon, $N = 4$.

$$\boldsymbol{U}[t, \lambda(t_0)] = \begin{cases} -\dfrac{B^T \Phi^{-T}(t, t_0)\boldsymbol{\lambda}(t_0)}{|B^T \Phi^{-T}(t, t_0)\boldsymbol{\lambda}(t_0)|} b, & |p(t)| > b \\ -B^T \Phi^{-T}(t, t_0)\boldsymbol{\lambda}(t_0), & |p(t)| \le b \end{cases} \quad (24)$$

where $\boldsymbol{\lambda}(t_0)$ is solved from Eq. (23). This result is compatible with Ref. 4.

Continuous Unbounded Controller

Because the bound is removed, the controller is

$$\boldsymbol{U}[t, \boldsymbol{\lambda}(t_0)] = -B^T \Phi^{-T}(t, t_0)\boldsymbol{\lambda}(t_0) \quad (25)$$

where $\boldsymbol{\lambda}(t_0)$ is solved from

$$\boldsymbol{\lambda}(t_0) = \tilde{\tilde{\boldsymbol{C}}}^{-1}(t)[\boldsymbol{y}_f + \tilde{\boldsymbol{n}}(t) - \Phi(t_f, t)\boldsymbol{y}(t)] \quad (26)$$

where

$$\tilde{\tilde{\boldsymbol{C}}}(t) = -\Phi(t_f, t_0) \int_t^{t_f} \Phi^{-1}(\tau, t_0) B B^T \Phi^{-T}(\tau, t_0)\, \mathrm{d}\tau$$

In this special case, $\boldsymbol{\lambda}(t_0)$ is solved explicitly, without the need for iteration. This solution can be used to get an initial guess for the iterative solution of $\boldsymbol{\lambda}(t_0)$ for the general cases (bounded and discrete control). The result for this special case is compatible with Ref. 3.

Iterative Algorithm for λ_0

The heart of the closed-loop control law is the determination of $\boldsymbol{\lambda}_0$ that fulfills Eq. (23). The scalar function $F[\boldsymbol{\lambda}(t_0)]$ describes the magnitude of the vector whose components are the deviations of the state vector (position and velocity) from the end condition at the final time. The value of $F[\boldsymbol{\lambda}(t_0)]$ is the upper limit for each component of the deviation vector. Solution of Eq. (23) is performed online, whenever new measurements are available. The function $F[\boldsymbol{\lambda}(t_0)]$ is characterized by a nonsmooth and multiminima surface that becomes more complicated when the number of feasible thrust levels decreases. A typical view of the function $F[\boldsymbol{\lambda}(t_0)]$ appears in Fig. 1. Figure 1 was produced by varying two components of λ_0, with all other components fixed. This particular view is compatible with the case of example 1, when only one feasible thrust level is applied, $N = 1$. When the number of thrust levels tends to infinity, and when the thrust is unbounded as well, the minimum problem becomes convex, and an analytical solution can be obtained. However, when discrete control levels are involved, the multiminima problem has to be solved by an iterative method. From our experience with N in the range of 1–10 thrust levels, the iterative solution of the multiminima problem usually becomes more difficult as the number of thrust levels decreases. Because this procedure must be implemented during the mission in real time, it is essential to find an iterative method that can efficiently and quickly converge to the global minimum, or at least to a sufficient one. The simulated annealing method appears to be efficient, both in the aspect of convergence potency and rate of convergence. This method and its implementation are described in the Appendix.

Numerical Examples

The preceding control law is demonstrated for two examples: 1) correction of satellite orbit around the moon and 2) interplanetary trajectory from Earth to Mercury.

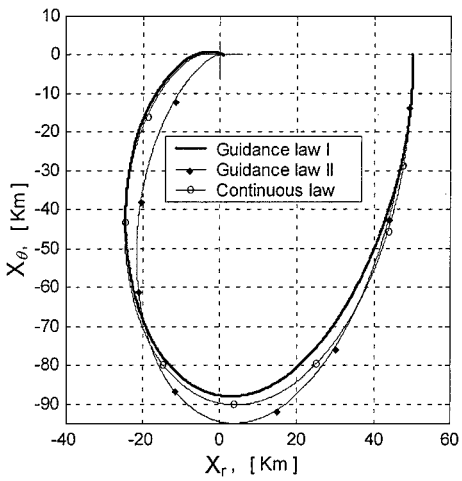

a) Position deviations

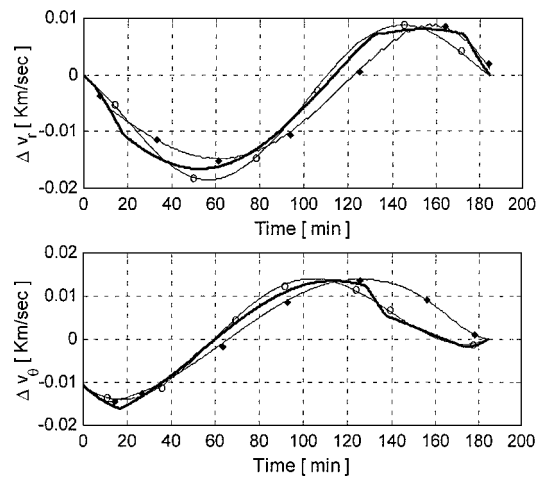

b) Velocity deviations

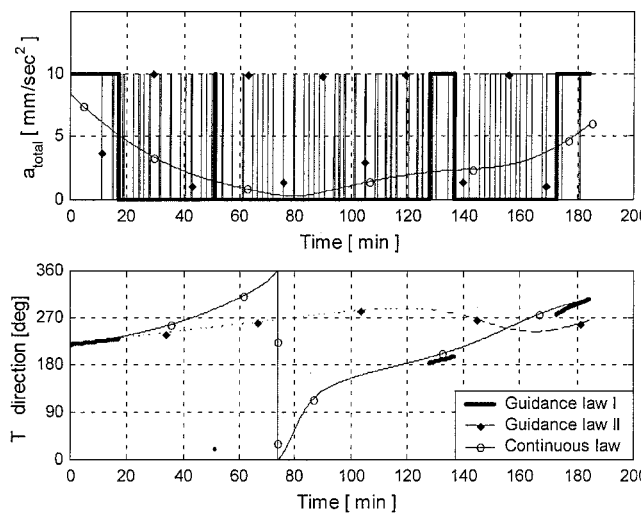

c) Control magnitude and direction

Fig. 4 Correction of satellite orbit around the moon, $N = 1$.

Example 1: Correction of Satellite Orbit Around the Moon

A satellite is orbiting the moon in a circular orbit at a radius of 3050 km. It is required to transfer to a circular orbit at a radius of 3000 km and meet the target orbit while accomplishing three-quarters of a circle. The required maneuver time is specified as three-quarters of the orbital period of the new orbit (about 185 min).

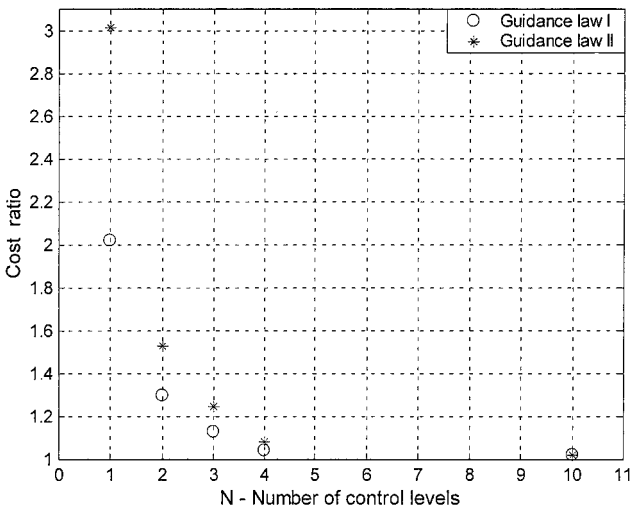

Fig. 5 Ratio between the achieved control cost and the optimal continuous control cost vs the number of control levels.

Because the terminal position, the terminal velocity, and the terminal time are specified, the problem is a rendezvous-type problem. Two control laws are presented: control law I is the iterative solution of $\boldsymbol{\lambda}(t_0)$ from Eq. (23) as explained earlier. This is a discrete optimal control law. Control law II is the use of the analytic solution (26) to $\boldsymbol{\lambda}(t_0)$ for the continuous case and then the fixing of the control value on the closest discrete value of the engine. The calculation is repeated each time a new state measurement is available. This is a suboptimal control law. In this example, there is no predetermined nominal transfer trajectory. The final trajectory is used as the nominal one.

Several simulations were performed for different numbers of thrust levels. The maximum thrust acceleration available was set to 10 mm/s^2. Figure 2 shows the results for $N = 10$. The trajectory deviations and the velocity deviations are shown in a coordinate system that is fixed with respect to a moving point on the final trajectory. At $t = 0$, the origin of this coordinate system is located on the final trajectory right below the satellite, on the same radius. The origin is moving at the orbital velocity of the final trajectory. The coordinates are $(\hat{r}, \hat{\theta})$, where $\hat{r}$ in the radial direction, pointing outward, and $\hat{\theta}$ is the circumferential direction. This kind of presentation is chosen to scale the deviations better and to emphasize the convergence of the satellite to the target. The measurement updates are available at time intervals of 2 min. Figures 3 and 4 show the simulations results for $N = 4$ and 1 (on–off controller). The results in Figs. 3 and 4 include both control laws for the multilevel engine, as well as the continuous control law, as a comparison. For such a single correction mission, the relative change of mass of the satellite is fairly negligible. To emphasize

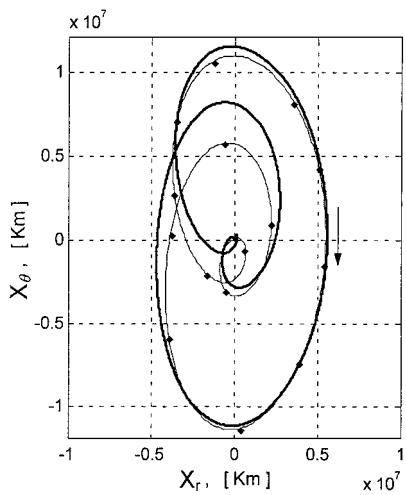

a) Position deviations

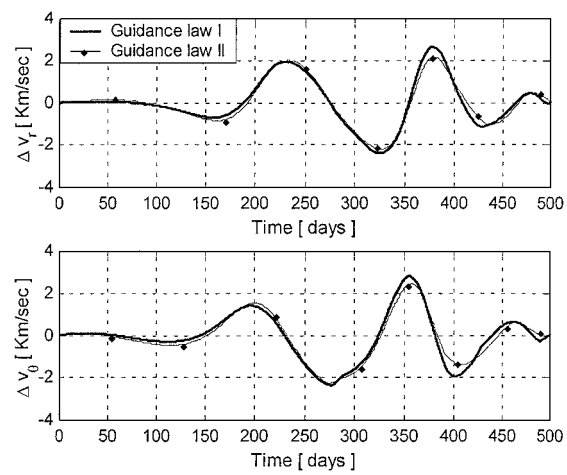

b) Velocity deviations

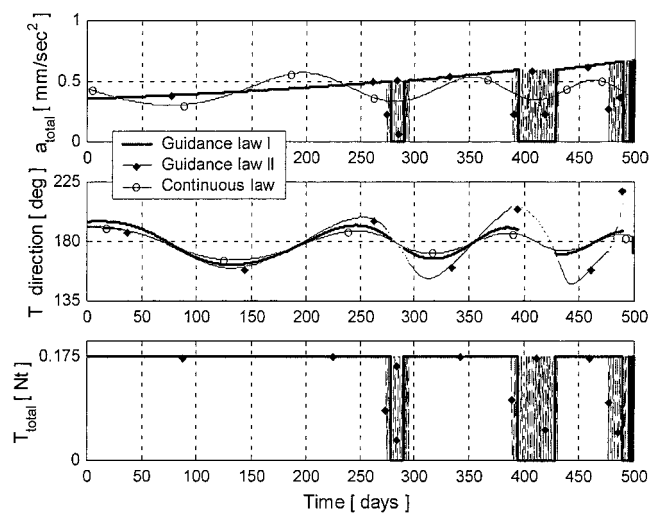

c) Applied thrust and acceleration

Fig. 6 Interplanetary trajectory from Earth to Mercury, $N = 1$.

Table 1 Comparison of performance for the transfer from Earth to Mercury[a]

Number of thrust levels	Control law	Fuel mass m_p, kg
1	I	233.5
	II	241.4
2	I	224.6
	II	228
3	I	222
	II	223.3
∞ Continuous	Optimal	220.2

[a]Here, $m_0 = 500$ kg.

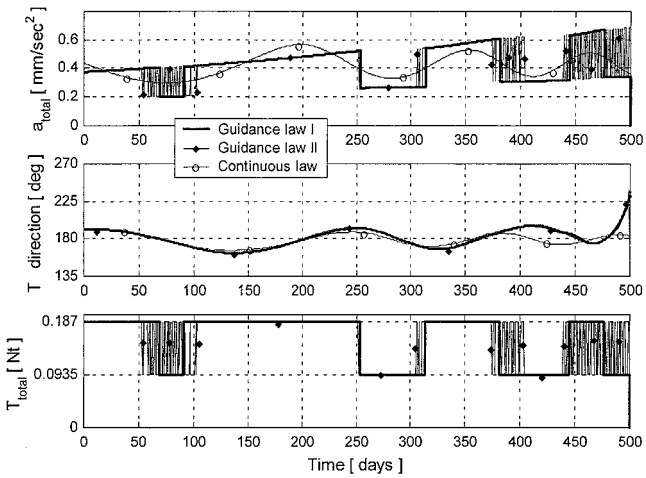

Fig. 7 Interplanetary trajectory from Earth to Mercury, the applied thrust and acceleration, $N = 2$.

the differences between the different control laws (optimal discrete law, suboptimal discrete law, and continuous law), the cost function

$$J_n = \int_{t_o}^{t_f} U^2 \, \mathrm{d}t$$

is used for comparison. The relative cost function for each control law, normalized to the continuous case cost function, is shown in Fig. 5, as a function of the number of thrust levels. The following observations are noted:

1) Both control laws perform well in the sense of guiding the satellite to the target point. The difference between the trajectories of the different control laws is negligible for large number of thrust levels.

2) The control acceleration produced by control law II tends to chatter when the continuous thrust is in between two thrust levels, whereas control law I is smoother.

3) The improvement (reduction) in the cost function of control law I (the more complex one) relative to control law II becomes higher as the number of thrust level decreases. For $N > 4$, the improvement (for this example) is negligible.

Example 2: Interplanetary Trajectory from Earth to Mercury

The spacecraft performs a maneuver from Earth to Mercury. The initial orbit is the Earth orbit around the sun, and the final one is Mercury's orbit around the sun. Both orbits are assumed to be circular. The transfer time is specified as 500 days.

For this example, the mass of the spacecraft changes significantly. Because the engine provides constant thrust levels, the thrust acceleration levels (which are the control variables) are not constant values. The available thrust accelerations are given by

$$|\boldsymbol{U}(t)| \in U_{b-N}(t) = T_{b-N}/m(t) \tag{27}$$

where $m(t)$ is the instantaneous mass of the spacecraft and is computed from the relationship

$$\dot{m}(t) = \frac{m^2(t)U^2(t)}{2P_{wr}} \tag{28}$$

The power of the engine was taken as $P_{wr} = 2.5$ kW and the initial mass as $m_0 = 500$ kg. For this mission, an optimal reference trajectory was computed by a series of successive calculations of control law I, when the initial guess was the continuous solution.

The results are shown in Figs. 6 (for $N = 1$) and 7 (for $N = 2$). Again note that control law I is smoother than control law II. As explained earlier in the development of the optimal control law, the controller toward the end of the trajectory may result in chatter, as seen in Figs. 6 and 7, but the chatter for the optimal control law is considerably shorter than for the suboptimal law.

The fuel mass for each maneuver is summarized in Table 1. Implementation of control law I is more fuel efficient, but the difference is negligible for $N > 2$.

Conclusions

In this research, we developed closed-loop controllers for the space maneuvering of spacecraft with electric propulsion systems, where the thrust is available in several discrete levels. The control law is developed using the neighboring trajectory method. Two control laws were developed. One is the discrete optimal control law, based on the iterative procedure. The other is a suboptimal control law, based on analog-to-digital conversion of the analytic solution of the continuous-unbounded controller. The latter is not optimal in the sense of fuel consumption but is easy to apply due to the low computational effort that it requires. The differences between the optimal discrete law, the suboptimal discrete law, and the continuous optimal law are mission dependent and are related to the available thrust levels and other factors such as mass of the spacecraft and power. For the demonstrated missions, by applying the discrete control laws, it appeared that few levels of control (more than four) are sufficient to obtain optimality that is very close to that achieved by the continuous optimal controller (theoretical). Furthermore, in that case (when more than four levels are feasible), the difference between the discrete optimal control law and the suboptimal control law are quite small, in the sense of fuel consumption, and the use of the latter should be considered.

When the number of feasible thrust levels is decreased, the advantage of the optimal guidance law is evident. In addition, control law I requires fewer switches than control law II. This can be important in real-life implementation, where high-frequency chatter may introduce increased thrust on–off uncertainties that degrade the overall performance.

An interesting result arises from the examination of the discrete optimal control law. In the problem of the transfer between two coplanar circular orbits, when only one level of control is feasible (bang–bang), the optimal solution appeared to coincide with the classic optimal two-impulse Hohmann transfer.

The numerical minimization was based on the simulated annealing method, which proved to be very effective.

With regard to the optimal discrete control law I, a practical issue is the possibility that the numerical iterative algorithm does not converge. In practice, at a specific point on the trajectory, the control cost can be bounded by the cost associated with the suboptimal control law II. The vector $\boldsymbol{\lambda}(t_0)$ that is analytically computed for control law II is used as an initial guess for the iterative algorithm of control law I; hence, the iterative algorithm improves the control cost even if there is no full convergence.

From the numerical examples it appears that, with control law I, convergence is slower when a few control levels are feasible (1–2 control levels). The convergence is usually accelerated as the number of control levels increases. Also, frequent updates of the measurements improve the convergence rate.

Appendix: Simulated Annealing Method

The method of simulated annealing is analogous to the way that liquids freeze and crystallize or metals cool and anneal. If a liquid cools down slowly, the atoms can form a pure crystalline structure, which is compatible with the system's minimum energy state. Along with this process, energy of the system decreases, but sometimes the energy must be temporarily increased to enable the system to proceed toward the global minimum. The optimization procedure that is involved with the annealing process[8] is based on Boltzmann probability distribution:

$$\text{prob}(E) \sim \exp[-E/(kT)]$$

This expression, which is applied to a system in thermal equilibrium at temperature T, represents the probability of being at a particular energy state E, among all possible energy states. Even at low temperature, there is a probability, albeit very small, for being in a high-energy state. Therefore, there is a corresponding probability for the system to get out of a local minimum energy in favor of finding a better, more global minimum.

The simulated annealing optimization in our case is based on the extension of the downhill simplex method. The detailed procedure can be found in Ref. 8. In this method, the single point λ_0 of dimension N, with the scalar value $F[\boldsymbol{\lambda}(t_0)]$, is replaced by a simplex of $N+1$ points. The simplex moves in the space of search, expanding and contracting, following new points as replacement points. At each step, a vertex of the simplex is replaced if a downhill step is obtained. The simplex is always proceeding downhill toward the nearest local minimum.

To extend the simplex algorithm and apply the simulated annealing procedure, a parameter T, which is equivalent to temperature in the natural process, is introduced. We add a positive logarithmically distributed random increment, proportional to the temperature T, to the stored function value $F(\boldsymbol{\lambda})$ associated with each vertex of the simplex, and we subtract a similar random variable from the function value of each new point that is tested as a replacement point. As before, the algorithm always accepts a true downhill step, but, sometimes, an uphill step is accepted. Indeed, the algorithm has a better chance to proceed uphill the function $F(\boldsymbol{\lambda})$, as the temperature increases. The solution of the minimum problem is initiated with high temperature T. The algorithm then is capable of climbing out of a local minimum, and proceeds toward a more global one. As the algorithm progresses and as the temperature is lowered, uphill steps become rare. When $T \to 0$, the algorithm is identical with the downhill simplex procedure and converges to the nearest minimum, which is supposed to be the global one.

Generally, the process of finding the global minimum can be a long one, and sometimes it may fail to converge. In our case, the procedure is applied whenever a new state measurement is available, to search for the global minimum or at least a sufficient one. It appears that, if the measurements are frequent enough, the multidimensional surface that represents the function $F(\boldsymbol{\lambda})$ is slightly changed between consequent measurements. In that case, the minimum from the previous iteration is likely to be close to the current one; hence, the convergence is fast. Experience of many simulations shows that the difficulties of solving the minimum problem appear mostly at the point of initiating the mission.

It must be emphasized that slow convergence of the solution, as well as some non-convergence along the mission, may increase the overall cost function, but does not affect the fulfillment of the final conditions.

References

[1]Williams, S. N., and Coverstone-Carroll, V., "Benefits of Solar Electric Propulsion for the Next Generation of Planetary Exploration Missions," *Journal of the Astronautical Sciences*, Vol. 45, No. 2, 1997, pp. 143–159.

[2]Marec, J. P., *Optimal Space Trajectories*, Elsevier Scientific, New York, 1979, pp. 7–12, 53–70, 89–118.

[3]Gipsman, A., Guelman, M., and Kogan, A., "Autonomous Navigation and Guidance System for Low Thrust Driven Deep Space Missions," 49th International Astronautical Congress, IAF-98-A.2.05, Sept. 1998; also *Acta Astronautica*, Vol. 44, Nos. 7–12, 1999, pp. 353–364.

[4]Carter, T. E., "Optimal Power-Limited Rendezvous of a Spacecraft with Bounded Thrust and General Linear Equations of Motion," *Journal of Optimization Theory and Applications*, Vol. 87, No. 3, 1995, pp. 487–515.

[5]Carter, T. E., and Pardis, C. J., "Optimal Power-Limited Rendezvous with Upper and Lower Bounds on Thrust," *Journal of Guidance, Control, and Dynamics*, Vol. 19, No. 5, 1996, pp. 1124–1133.

[6]Raitses, Y., "Investigations of the Hall Thruster and Its Use for Satellite Drag Compensation," Sc.D Dissertation, Faculty of Aerospace Engineering, Technion—Israel Inst. of Technology, Haifa, Israel, Oct. 1997.

[7]Bryson, A. E., and Ho, Y. C., *Applied Optimal Control*, Hemisphere, Washington, DC, 1975, pp. 212–243.

[8]Press, W. H., Teukolsky, S. A., Vetterling, W. T., and Flannery, B. P., "Numerical Recipes in C," *The Art of Scientific Computing*, 2nd ed., Cambridge Univ. Press, Cambridge, England, U.K., 1992, pp. 394–444.